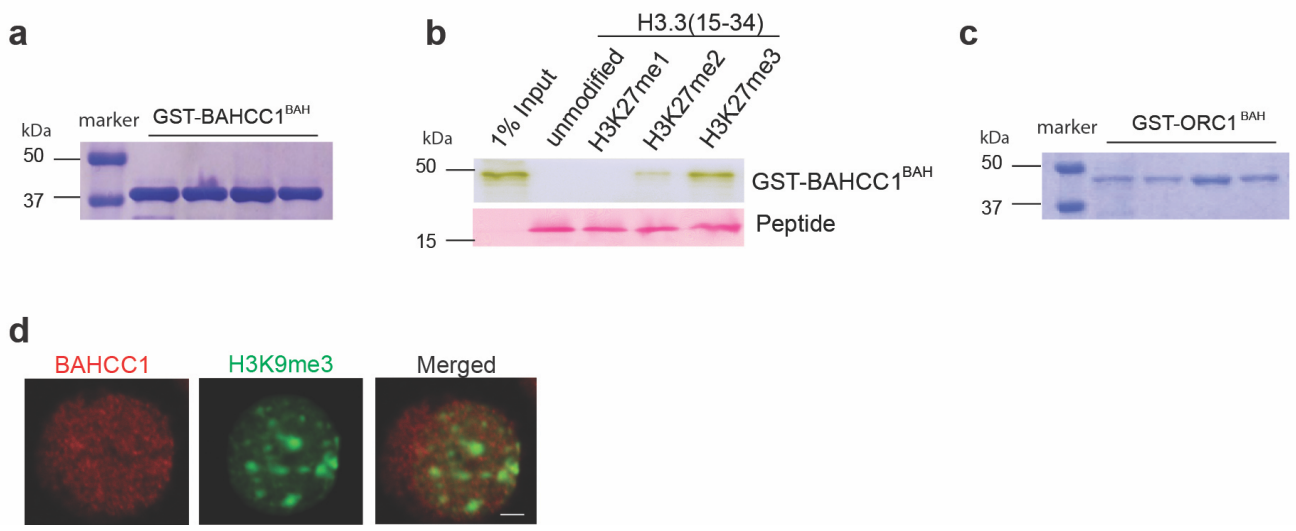

Supplementary Fig 1. The BAH domain of BAHCC1 (BAHCC1^{BAH}) is an H3K27me3/2-specific 'reader' in mammalian cells.

a, Coomassie blue staining of the purified BAHCC1^{BAH} recombinant protein fused to GST.
b, Representative silver staining of input (lane 1) and pulldown samples (lanes 2-5 of the top panel) using the GST-BAHCC1^{BAH} recombinant protein and the histone H3.3 peptide (amino acids 15-34) harboring non-, mono-, di-, or tri-methylated lysine 27 (ponceau red staining image of peptides shown at the bottom).
c, Coomassie blue staining of the purified ORC1^{BAH} recombinant protein fused to GST.
d, Representative images of confocal immunofluorescence microscopy showing that BAHCC1 (red) does not colocalize with H3K9me3 (green) in JURKAT cells. Scale bar, 2 μm.

Supplementary Fig. 2

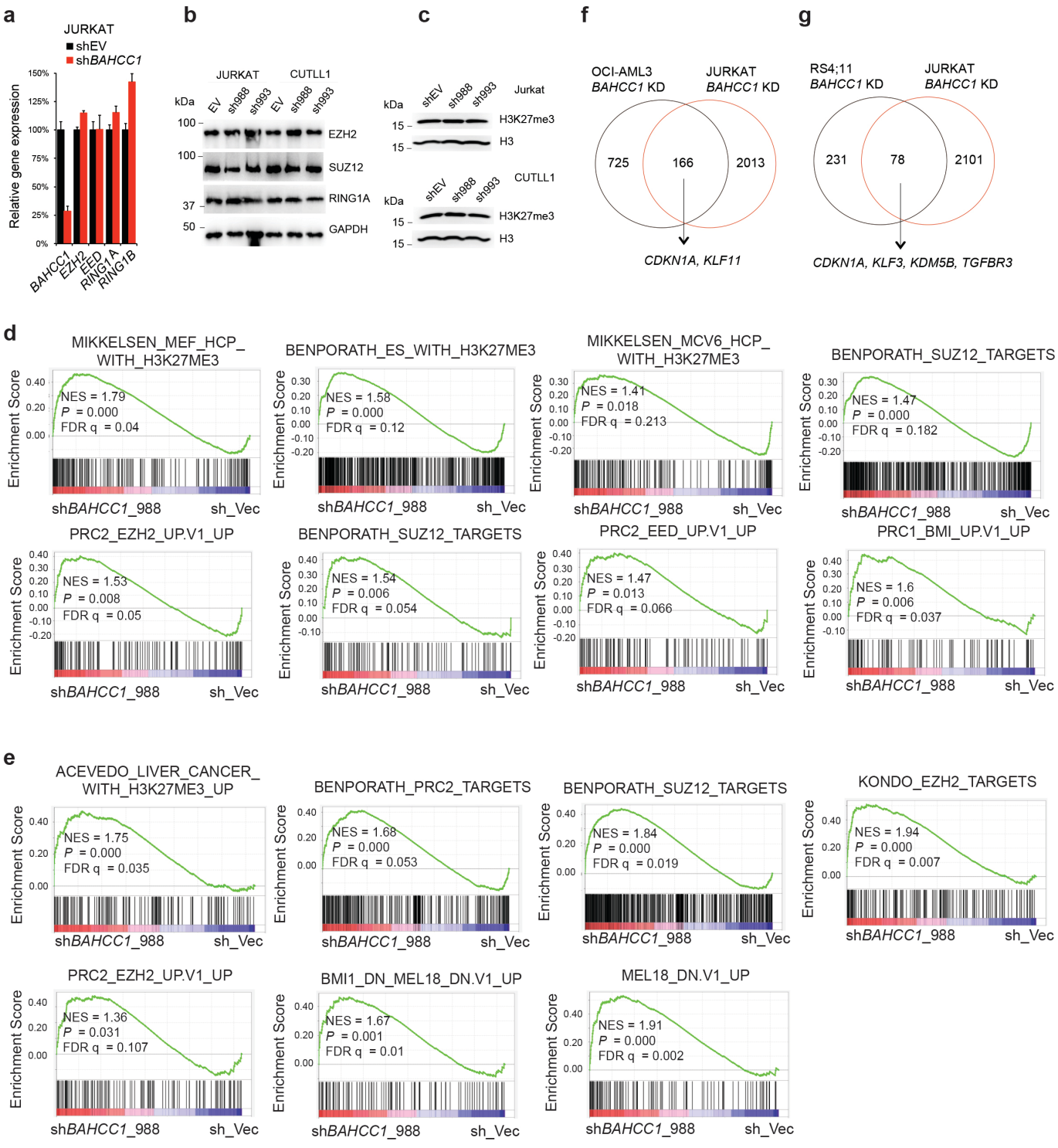

Supplementary Fig 2. RNA-seq based transcriptome profiling reveals the gene-expression programs regulated by *BAHCC1* in various human acute leukemia models.

a-**b**, The mRNA and protein levels of the indicated PRC1 or PRC2 component after *BAHCC1* knockdown (KD) relative to mock empty vector control (shEV), as examined by RT-qPCR (panel **a**; n=3 biologically independent samples, with data presented as mean values ± SD) and western blot (panel **b**), respectively, in JURKAT (panel **a** and **b**, left) and CUTLL1 (panel **b**, right) T-ALL cells.

c, Immunoblotting of H3K27me3 and total H3 in JURKAT and CUTLL1 cells after stable KD of *BAHCC1* (using either sh988 or sh993), relative to shEV control.

d-e, GSEA using the RNA-seq profiles of OCI-AML3 AML (panel **d**) and RS4;11 B-ALL (**e**) cells shows that, relative to mock vector control (sh_Vec), BAHCC1 depletion is positively correlated to derepression of the indicated gene signatures related to H3K27me3, PRC1 or PRC2 in both acute leukemia models.

f, Venn diagram illustrating the overlap of differentially expressed genes (DEGs) found to be upregulated after *BAHCC1* depletion, relative to mock, in the OCI-AML3 (black) and JURKAT (red) cells.

g, Venn diagram illustrating the overlap of DEGs found to be upregulated after *BAHCC1* depletion, relative to mock, in the RS4;11 (black) and JURKAT (red) cells.

a

	BAH(Y2533A) vs WT		BAH(W2554G) vs WT	
MSigDB Gene Set	*P*-value	Adjusted *P*	*P*-value	Adjusted *P*
Polycomb-related				
MEISSNER_BRAIN_HCP_WITH_H3K4ME3_AND_H3K27ME3	4.72E-34	8.35E-31	3.09E-29	3.42E-26
NUYTTEN_EZH2_TARGETS_UP	6.89E-19	2.10E-16	4.33E-26	2.40E-23
BENPORATH_ES_WITH_H3K27ME3	9.45E-19	2.70E-16	3.40E-03	1.53E-02
BENPORATH_SUZ12_TARGETS	1.43E-13	1.46E-11	2.60E-02	7.55E-02
BENPORATH_EED_TARGETS	1.59E-09	8.07E-08	2.52E-03	1.20E-02
DOUGLAS_BMI1_TARGETS_UP	2.38E-07	6.88E-06	8.15E-12	3.36E-10
MIKKELSEN_NPC_HCP_WITH_H3K27ME3	1.46E-06	3.38E-05	9.73E-03	3.58E-02
Differentiation-related				
GO_NEUROGENESIS	5.67E-24	3.14E-21	4.13E-15	3.21E-13
GO_REGULATION_OF_CELL_DIFFERENTIATION	2.04E-20	7.87E-18	3.38E-21	6.95E-19
GO_CELL_DEVELOPMENT	1.15E-17	2.82E-15	9.00E-16	7.83E-14
GO_POSITIVE_REGULATION_OF_MULTICELLULAR_ORGANISMAL_PROCESS	6.99E-16	1.38E-13	6.89E-14	4.30E-12
GO_TISSUE_DEVELOPMENT	1.10E-13	1.17E-11	6.28E-22	1.46E-19
GO_EPITHELIUM_DEVELOPMENT	5.06E-13	4.92E-11	2.69E-15	2.17E-13
GO_POSITIVE_REGULATION_OF_DEVELOPMENTAL_PROCESS	2.56E-12	2.20E-10	1.79E-16	1.94E-14
GO_NEGATIVE_REGULATION_OF_MULTICELLULAR_ORGANISMAL_PROCESS	1.10E-11	8.70E-10	2.30E-12	1.11E-10
GO_ANATOMICAL_STRUCTURE_FORMATION_INVOLVED_IN_MORPHOGENESIS	2.65E-10	1.51E-08	5.56E-17	6.40E-15
GO_POSITIVE_REGULATION_OF_CELL_DIFFERENTIATION	2.72E-09	1.27E-07	4.61E-16	4.58E-14
GO_EMBRYO_DEVELOPMENT	6.89E-08	2.29E-06	1.28E-13	7.44E-12
GO_DEVELOPMENTAL_MATURATION	7.03E-08	2.33E-06	8.05E-05	6.71E-04
GO_BLOOD_VESSEL_MORPHOGENESIS	7.97E-08	2.62E-06	1.16E-16	1.30E-14
GO_ORGAN_MORPHOGENESIS	1.50E-06	3.45E-05	1.41E-13	8.13E-12
ADDYA_ERYTHROID_DIFFERENTIATION_BY_HEMIN	5.66E-06	1.10E-04	1.28E-19	2.10E-17
Cell death related				
GRAESSMANN_APOPTOSIS_BY_DOXORUBICIN_UP	9.14E-19	2.70E-16	5.67E-19	8.66E-17
GO_REGULATION_OF_CELL_DEATH	2.63E-12	2.24E-10	6.31E-16	5.88E-14
Others				
HELLER_HDAC_TARGETS_UP	2.64E-15	4.04E-13	6.50E-22	1.48E-19
SENESE_HDAC1_TARGETS_UP	3.02E-14	1.82E-12	9.79E-19	1.38E-16

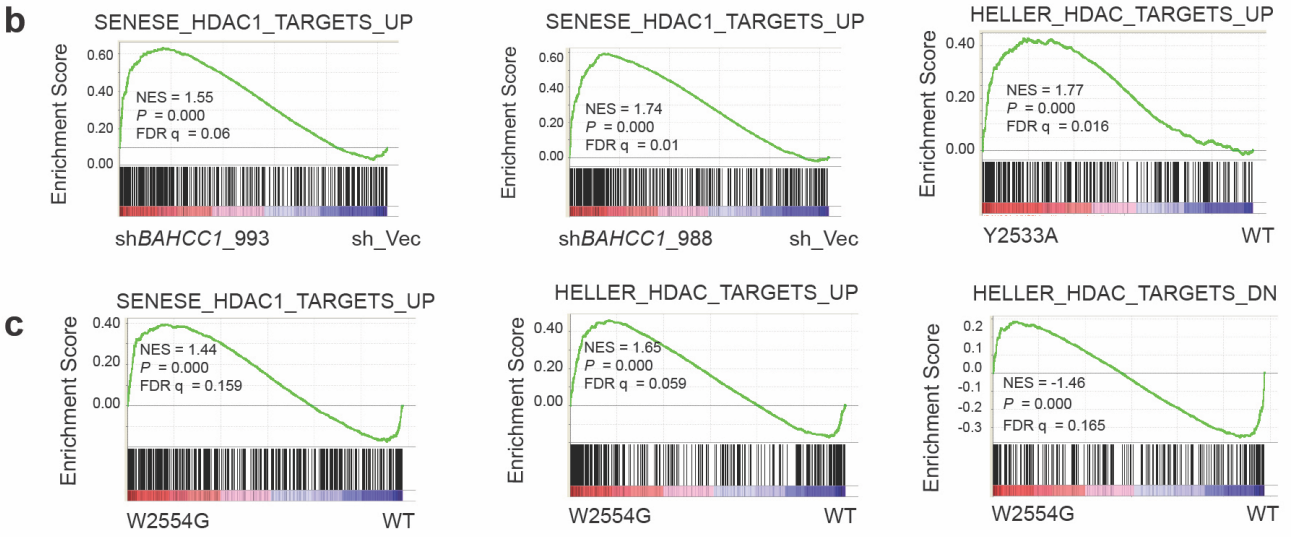

Supplementary Fig 3. The H3K27me3-binding-defective mutation of *BAHCC1*^{BAH} causes derepression of H3K27me3 target genes in acute leukemia cells.

a, Summary of Platform for Integrative Analysis of Omics data (Piano) analyses, which show significant enrichment of the indicated gene sets in JURKAT cells with either the Y2533A (left) or W2554G (right) homozygous mutation of *BAHCC1*^{BAH}, relative to the matched WT cells.

b-c, GSEA revealing the positive correlation of *BAHCC1* depletion (**b**), or the Y2533A or W2554G homozygous mutation of *BAHCC1*^{BAH} (**b-c**), with reactivation of the *HDAC* target gene signatures.

Supplementary Fig 4. A germline mutation of *Bahcc1*^{Y2537A} in mice causes phenotypes of partially penetrant neonatal lethality and mild dwarfism, while not significantly affecting adult hematopoiesis in the surviving adult mice.

a-c, Representative flow cytometry plots to profile the indicated blood cell lineages in the bone marrow (**a**) or spleen (**b**), as well as the indicated HPSC compartments in the bone marrow (**c**) of the six-month-old littermates with either WT or the Y2537A homozygous mutation of *Bahcc1*^{BAH}. The gating strategy of flow cytometry was shown in the top panel.

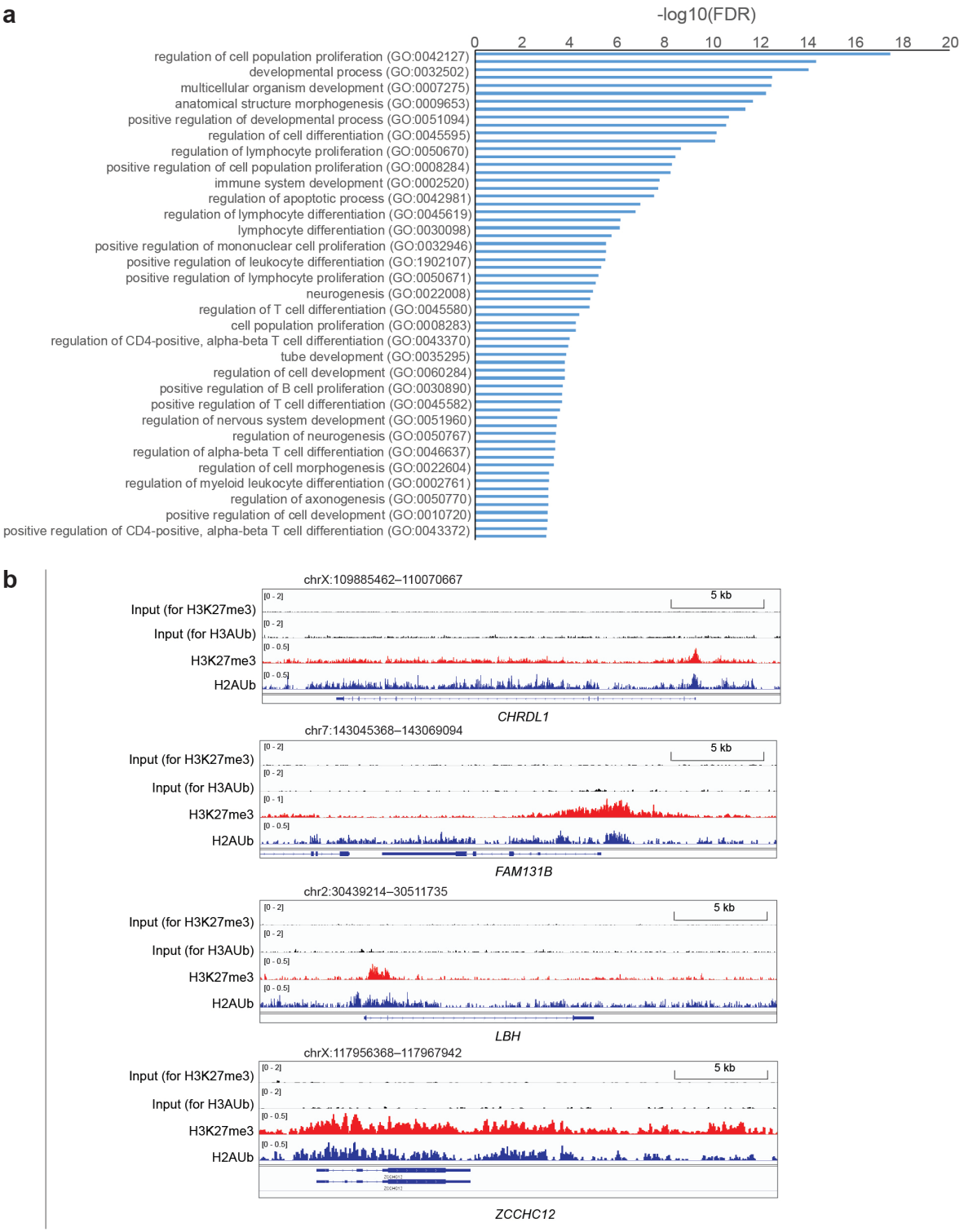

Supplementary Fig 5. An E2A-PBX1-transformed murine acute leukemia model, established with HSPCs from either WT or *Bahcc1*^{Y2537A}-mutated mice, reveals a positive correlation between the H3K27me3-binding-defective Y2537A mutation of *Bahcc1*^{BAH} and derepression of the H3K27me3/Polycomb target genes.

a, GO analyses of the genes upregulated in the E2A-PBX1-transformed murine leukemia cells with the Y2537A homozygous mutation of *Bahcc1*^{BAH}, relative to WT.

b, ChIP-seq profiles of H3K27me3 and H2AK119 ubiquitination (H2Aub) at the indicated BAHCC1- and PRC1-corepressed genes in 293 cells.